RSC Advances

ROYAL SOCIETY OF CHEMISTRY

www.rsc.org/advances

ZnO coated $CoFe_2O_4$ Nanoparticles for Multimodal Bio-Imaging

N Venkatesha[1], Yasrib Qurishi[3], Hanudatta S. Atreya[2], Chandan Srivastava[1*]

[1]Department of Materials Engineering, Indian Institute of Science, Bangalore, India
[2]NMR Research Centre, Indian Institute of Science, Bangalore, India
[3]Department of Molecular Reproduction, Development and Genetics, Indian Institute of Science, Bangalore, India

*Corresponding Author: Email: csrivastava@materials.iisc.ernet.in
Phone: 91-080-22932834
Fax: 91-080-2360 0472

Abstract

Potential of $CoFe_2O_4$-ZnO core-shell nanoparticles for fluorescence optical imaging and as a contrast agent for magnetic resonance imaging (MRI) is demonstrated. Two different core-shell $CoFe_2O_4$-ZnO nanoparticle geometries were produced by the wet chemical synthesis method. In one case, the core-shell geometry was made up of individual nanoparticles containing $CoFe_2O_4$ as core and ZnO as shell whereas in the other case, agglomerates of $CoFe_2O_4$ nanoparticles were encapsulated within ZnO capsules. It was observed that the $CoFe_2O_4$-ZnO core-shell nanoparticles with a unique geometry in which $CoFe_2O_4$ ferrite nanoparticles agglomerates were present within ZnO capsules yielded a very high value of transverse proton relaxivity (264.6 $mM^{-1}s^{-1}$) when compared to the transverse proton relaxivity exhibited by the individual core-shell nanoparticles (31.8 $mM^{-1}s^{-1}$). Using HeLa cells to which the core-shell nanoparticles were attached, it is shown that the $CoFe_2O_4$-ZnO nanoparticle can also be used as contrast agents in fluorescence imaging. As-synthesized $CoFe_2O_4$-ZnO core-shell nanoparticles were also found to exhibit biocompatibility towards the MCF-7 cell line. Taken together, this opens up new avenues for superparamagnetic ferrite based nanoparticles in bio-imaging applications.

Keywords: $CoFe_2O_4$-ZnO, Core-Shell Nanoparticles, Magnetic Resonance Imaging, Fluorescence Imaging.

1. Introduction

A complete bio-imaging routine for diagnosis today involves application of different imaging modalities such as magnetic resonance imaging (MRI), positron emission tomography (PET), computed X-ray tomography (CT) etc.[1,2] Apart from their unique advantages, each technique suffers from specific limitations owing to which use of more than one imaging modality is necessary for achieving a set of desired attributes such as high spatial resolution, target specificity, high detection sensitivity, real-time imaging etc.[3] For instance, even though MRI and CT techniques offer high imaging resolution they suffer from low detection sensitivity.[4] To enhance the detection sensitivity, PET, which is a radioactive imaging technique having high detection sensitivity is additionally used. PET, however, is limited by its poor imaging resolution, which are the strengths of the MRI and CT techniques.[5] Multi-modal imaging necessitates the injection of several types of image contrast enhancing agents into the human body for examination.[6,7] To reduce the dosage of different types of contrast agents, studies have focused on designing contrast agents which are capable of enhancing contrast in multiple imaging modalities. Some interesting developments made in this direction are: (a) doping of fluorescent quantum dots with paramagnetic ions, (b) composite of fluorescent dyes and paramagnetic Gd^{3+} chelates, (c) γ-ray nucleotide conjugated with optical fluorescence dyes or paramagnetic agents etc.[8–13]

In this paper, we demonstrate the potential of chemically synthesized $CoFe_2O_4$-ZnO core-shell nanoparticles as a contrast agent in MRI and fluorescence imaging. Several methods have been reported for the synthesis of superparamagnetic ferrite based nanoparticles by the

researchers.[14-16] Ferrite based nanoparticles have also been widely explored for their potential application as contrast agent in MRI.[17,18] The previous studies include synthesis and investigation of $CoFe_2O_4$ nanoparticles for MRI contrast agent application.[19] On the other hand, ZnO nanoparticles have been explored for biomedical applications like fluorescence imaging and bio-sensing.[20] The optical properties of ZnO nanoparticles can be tuned by varying its size or by doping it with elements like Mn, Gd and Eu.[21] Coating of ferrite nanoparticles with ZnO therefore renders the $CoFe_2O_4$-ZnO core-shell nanoparticles both magnetically and optically active as shown in the present study. This study also illustrates the effect of two different core-shell geometries of fluorescent $CoFe_2O_4$-ZnO core-shell nanoparticles on the transverse relaxivity value of protons in the dispersion of these nanoparticles.

2. Experimental

2.1. Synthesis

A two-step methodology was used to synthesize $CoFe_2O_4$-ZnO core-shell nanoparticles. In the first step, $CoFe_2O_4$ seed nanoparticles were synthesized and in the second step ZnO phase was grown over the seeds to produce $CoFe_2O_4$-ZnO core-shell nanoparticles.

2.2.1 Synthesis of $CoFe_2O_4$ seed nanoparticles

To synthesize $CoFe_2O_4$ seed nanoparticles, $Co(acac)_2$ (1 mmol), $Fe(acac)_3$ (2 mmol), 1,2-hexadecanediol (5 mmol), oleic acid (6 mmol), and oleylamine (6 mmol) and diphenyl ether (20 mL) were mixed together. This solution was then poured into a three neck round bottom flask fitted with a magnetic stirrer and a reflux condenser. The reaction mixture was heated to 150˚C and kept at this temperature for 30 min. Temperature of the reaction mixture was then raised to its reflux temperature and maintained there for 60 min. After 60 min, the reaction mixture containing precipitated nanoparticles was cooled down to the room temperature. The whole

synthesis reaction was carried out in argon atmosphere. At the room temperature, 40 mL of ethanol was added into the reaction mixture to sediment the nanoparticles which were subsequently isolated by centrifugation.

2.2.2 Synthesis of $CoFe_2O_4$-ZnO core-shell nanoparticles

To synthesize $CoFe_2O_4$-ZnO core-shell nanoparticles, 40 mg of as-synthesized $CoFe_2O_4$ seed nanoparticles were dispersed in 20 mL hexane by sonication. Into this dispersion, 20 mL benzyl ether, 6 ml oleic acid, 6 ml oleylamine were added. This reaction mixture was then transferred into a three neck round bottom flask fitted with a magnetic stirrer and a reflux condenser. The reaction mixture was heated to 100°C and kept at this temperature for 60 min to evaporate away the hexane. After 60 min, $Zn(acac)_2$ (3 mmol) was added into the reaction mixture. The reaction mixture was then heated to 290°C and kept at this temperature for 60 min. After 60 min of reflux the reaction mixture containing precipitated nanoparticles was cooled down to the room temperature. 40 mL ethanol was then added into the reaction mixture to sediment the nanoparticles which were subsequently isolated by centrifugation. Isolated nanoparticles were then washed several times for further characterization.

2.2.3 Synthesis of *modified* $CoFe_2O_4$-ZnO core-shell nanoparticles.

To synthesize modified $CoFe_2O_4$-ZnO core-shell nanoparticles, 40 mg of as-synthesized $CoFe_2O_4$ seed nanoparticles were dispersed in 20 mL of hexane by sonication. Into this dispersion, 20 mL of benzyl ether and 6 ml oleylamine were added. This reaction mixture was then transferred into a three neck round bottom flask equipped with a magnetic stirrer and a reflux condenser. This reaction mixture was heated to 100 °C and kept at this temperature for 60 min. After 60 min, $Zn(acac)_2$ (3 mmol) was added into the reaction mixture. The temperature of the reaction mixture was then increased to 290 °C and maintained for 60 min. After 60 min of

reflux the reaction mixture containing precipitated nanoparticles was cooled down to the room temperature. 40 mL ethanol was then added into the reaction mixture to sediment the nanoparticles which were subsequently isolated by centrifugation.

2.3 Coating of nanoparticles with chitosan

Uniform dispersion of nanoparticles in water is essential for bio-medical applications. To make the nanoparticles water dispersible, a surfactant exchange reaction was conducted in which oleyl amine and oleic acid on the nanoparticle surface were replaced by chitosan.[22] Chitosan (β-(1-4)-linked D-glucosamine (deacetylated unit) and N-acetyl-D-glucosamine(acetylated unit)) is a biocompatible polymer which has been tested widely for various bio-medical applications.[23] For the ligand exchange reaction, 50 mg of nanoparticles was dispersed in 20 ml of hexane by sonication. A solution was prepared by dissolving DMSA (2,3-dimercaptosuccinic acid) into DMSO (dimethyl sulfoxide) in 10 (w/v) % ratio. Into this solution, the nanoparticle dispersion was added in 1:1 ratio by volume and sonicated for 1 h. Hexane layer containing organic precursors was then discarded by using the separating funnel. DMSA coated water soluble nanoparticles were then dispersed in DMSO. The nanoparticles were then washed using DI water and isolated by magnetic separation. Chitosan solution was prepared by dissolving 0.5 g of chitosan in a 2.0 % aqueous acetic acid solution by magnetic stirring for 30 min. 5 mL of this solution was then added into the aqueous dispersion containing DMSA-coated nanoparticles and sonicated for 1 h. During the sonication, chitosan got electrostatically attached to the nanoparticle surface. Into this dispersion, 50 mg of EDC [1-ethyl-3-(3-dimethylaminopropyl) carbodiimide hydrochloride] was then added and sonicated for further 2 hours. EDC reacted with DMSA carboxyl groups on the surface of the nanoparticles to form an amine reactive O-acylisourea intermediate. This intermediate reacted with the amine group of chitosan yielding

water stable chitosan coated nanoparticles. Finally, this sample was washed with water followed by magnetic separation.

2.4 Characterization

X-ray diffraction (XRD) profiles were obtained from the as-synthesized samples using the X-Pert PAN Analytical machine employing Cu K-alpha radiation source. A 300 keV field emission FEI Tecnai F-30 transmission electron microscope (TEM) was used for obtaining TEM bright field images and selected area electron diffraction (SAD) patterns from as-synthesised samples. Samples for the TEM based analysis were prepared by drop-drying a highly dilute dispersion of the as-synthesised nanoparticles onto an electron transparent carbon coated Cu grid. Magnetic charaterization of the samples was done using the Lakeshore vibrating sample magnetometer (VSM). Concentration of iron in dispersions used for the MRI experiment was calculated by atomic absorption spectroscopy (AAS) technique conducted using the Thermo Electron Corporation M-series machine. X-ray photoelectron spectroscopy (XPS) profiles were obtained from the as-synthesized samples using an AXIS Ultra DLD (KRATOS ANALYTICAL) instrument. Transverse relaxivity of water protons in the presence of as-synthesized composites was measured using Bruker Avance-III spectrometer operating at 400 MHz ^{1}H resonance frequency. The transverse relaxation of water was measured using CPMG/T_2-filter (Carr Purucell Meiboom Gill) NMR experiment.[24] The relaxation delay time 'τ' was varied between 10 ms to 1 s collecting 12 data points to obtain the decay curve to extract T_2 relaxation time constant. The 16 K complex points were collected with 1.1 s acquisition time and 7000 Hz spectral width. The relaxation delay of 15 s was given between the scans. Perkin Elmer Lambda 35 UV-VIS spectrometer was used to obtained the UV-Vis absorption spectrum. Perkin Elmer LS50 B Luminescence Spectrometer was used to obtain the photoluminescence (PL) spectrum.

For the cytotoxicity analysis, MCF-7 (human breast cancer cells) cells were cultured in DMEM (Dulbecco's Modified Eagle's Medium) with 10% fetal bovine serum and incubated in a humidified atmosphere at 37 $^{\circ}$C with 5% CO_2. MTT assay was performed to evaluate the cytotoxicity of the chitosan coated nanoparticles. Cells were seeded at optimum density into each well of a 96-well plate and exposed to varied concentrations of chitosan coated core-shell nanoparticles. The cells were then incubated with the chitosan coated core-shell and modified $CoFe_2O_4$-ZnO core-shell nanoparticles for 24 h. 5 mg/mL MTT dye was then added into each well followed by further incubation for 3-4 h. The MTT formazon crystals formed are metabolically reduced by the mitochondria in viable cells to a colored formazon product, the intensity of which was measured spectrophotometrically in a plate reader at 570 nm.

To investigate the capability of core-shell and modified $CoFe_2O_4$-ZnO core-shell nanoparticles as possible contrast agents for fluorescence imaging, HeLa cells were selected. The cell lines were incubated with 2 ml of 50 micro molar core-shell and modified $MnFe_2O_4$-ZnO core-shell nanoparticles for 2 hours under standard conditions. The samples were dropped on a glass slide and fluorescence images were recorded by exciting the sample using white light.

3. Results and Discussion

SEM-EDS compositional analysis of $CoFe_2O_4$ seeds, $CoFe_2O_4$-ZnO core-shell and modified $CoFe_2O_4$-ZnO core-shell nanoparticles revealed the presence of Co, Fe and Zn elements in them. Representative SEM-EDS profiles are provided in Fig. 1. XRD profiles obtained from seed nanoparticles, core-shell and modified core-shell nanoparticles are shown in Fig. 2. The XRD curve obtained from the seed nanoparticles reveal diffraction peaks corresponding only to the $CoFe_2O_4$ phase.[25] Whereas, the XRD profile obtained from the core-

shell and modified core-shell $CoFe_2O_4$-ZnO nanoparticles reveal peaks corresponding to the $CoFe_2O_4$ phase and hexagonal ZnO phase.[26]

TEM bright field image of $CoFe_2O_4$ seed nanoparticles provided in Fig. 3(a) reveal that the first step of the synthesis process produced nearly spherical nanoparticles. SAD pattern obtained from the seed nanoparticles showing the presence of diffraction rings corresponding only to the ferrite phase is also provided in Fig. 3(a). Average size of the seed nanoparticles obtained from the summation average of sizes of 500 individual nanoparticles was 8.3±0.9 nm. Histogram showing the distribution of nanoparticle sizes is provided in Fig. 3(b). TEM bright field image of $CoFe_2O_4$-ZnO core-shell nanoparticles is shown in Fig. 3(c). High resolution TEM (HRTEM) image of a representative $CoFe_2O_4$-ZnO core-shell nanoparticle is shown as insert in Fig. 3(c). Difference in image contrast between the core and the shell phases is clearly visible in HRTEM image in Fig. 3(c). Average size of the core-shell nanoparticles obtained from the summation average of sizes of 500 individual nanoparticles was 11.6±1.8 nm. Histogram illustrating the distribution in sizes of core-shell nanoparticles is provided in Fig. 3(d). SAD pattern obtained from the $CoFe_2O_4$-ZnO core-shell nanoparticles showing the presence of diffraction rings corresponding to both ferrite and hexagonal ZnO phase are shown in Fig. 3(e).[27] Narrow distribution in nanoparticle sizes and presence of negligible number of nanoparticles with sizes ~8 nm in the histogram in Fig. 3(d) clearly shows that the reaction conditions adopted in the second step of the synthesis process led to uniform coating of the seed nanoparticles to form uniform core-shell nanoparticles. Core-shell geometry of the nanoparticles produced after the second step of the synthesis process was also confirmed by compositional line profile analysis of individual core-shell nanoparticles. Fig. 3(f) shows the scanning transmission electron microscopy-high angle annular dark field (STEM-HAADF) image of a representative

core-shell nanoparticle. The red line on the nanoparticle image is the path along which the compositional data was obtained using an electron probe of ~1.5 nm size. The compositional profile (distance vs. counts) obtained for the Co and Fe atoms shown in Fig. 3(g) and (h) shows an abrupt increase in the EDS signal in the middle of the nanoparticles showing that the core of the core-shell nanoparticles contains $CoFe_2O_4$ phase.

Representative low magnification and high magnification TEM bright field image of modified $CoFe_2O_4$-ZnO core-shell nanoparticles is provided in Fig. 4(a) and (b) respectively. It can be observed that the modification of the second step of the synthesis process has produced a different core-shell geometry in which agglomerates of $CoFe_2O_4$ nanoparticles are present inside hollow spherical capsules. SAD pattern obtained from the capsule containing nanoparticle is shown in Fig. 4(c). The SAD pattern in Fig. 4(c) predominantly reveals diffraction rings corresponding to the ferrite phase.[28] SAD pattern obtained from a capsule containing very less number of nanoparticles is shown in Fig. 4(d). The SAD pattern in Fig. 4(d) shows diffraction spots corresponding to single crystalline ZnO oriented along the [0001] zone axis.[29] The bright field image and electron diffraction analysis clearly confirmed that the second stage of the synthesis process has produced spherical ZnO capsules containing $CoFe_2O_4$ nanoparticle agglomerate. The STEM-HAADF image of ZnO capsule containing nanoparticle agglomerates and the EDS profile obtained from area scan are shown in Fig. 4(e) and (f) respectively. The EDS profile was obtained from the marked region in the Fig. 4(e). The presence of peaks corresponding to Fe, Co and Zn in the EDS profile again confirmed the presence of ZnO capsules containing $CoFe_2O_4$ nanoparticle agglomerate.

XPS based analysis of the modified $CoFe_2O_4$-ZnO core-shell nanoparticles was conducted. Fig. 5(a-c) respectively shows the XPS spectrum of Co2p, Fe2p and Zn2p obtained

from the modified core-shell nanoparticles. The Co 2p spectrum (Fig. 5(a)) shows two peaks at ~780 and 795 eV which are in accordance with the reported values for Co.[30] The Fe 2p spectrum (Fig. 5(b)) shows two peaks corresponding to $Fe2p_{3/2}$ and $Fe2p_{1/2}$ at ~710 and 725 eV revealing the presence of ferrite phase. Zn2p spectrum (Fig. 5(c)) shows two peaks at around 1023 and 1045 eV values which corresponds to Zn^{2+} in ZnO phase.[31]

Magnetic hysteresis curves obtained from $CoFe_2O_4$ seeds, core-shell and modified core-shell $CoFe_2O_4$-ZnO nanoparticles are shown in Fig. 6. Magnetic hysteresis curves were obtained at the room temperature using an applied field that varied in the range of 0-2 tesla. The magnetic hysteresis curves for $CoFe_2O_4$ seeds, $CoFe_2O_4$-ZnO core-shell and $CoFe_2O_4$-ZnO modified core-shell nanoparticles revealed negligible coercivity and no magnetic saturation till 2 tesla applied field. Both these attributes indicated that the as-synthesized seed, core-shell and modified $CoFe_2O_4$-ZnO core-shell nanoparticles are superparamagnetic in nature. Saturation magnetization values obtained for the seed, core-shell and modified core-shell nanoparticles were 55.7, 21.8 and 23.93 emu/g respectively. It can be observed that the presence of non-magnetic ZnO over $CoFe_2O_4$ has resulted in decreased value of saturation magnetization.

The chitosan coated seeds, core-shell and modified core-shell nanoparticles were diluted to four different concentrations. The iron concentration of the dispersion was determined using AAS (Atomic Absorption Spectroscopy). The T_2 values of the protons in the dispersion of these nanoparticles were determined by spin-echo method using 400 MHz NMR. The $1/T_2$ vs. iron concentrations plots for $CoFe_2O_4$ seed, core-shell and modified $CoFe_2O_4$-ZnO core-shell nanoparticles are shown in Fig. 7(a-c). Transverse relaxivity (r_2) values were determined from the slope of the linear fit to the data points in $1/T_2$ vs. Fe concentration plot. The r_2 values obtained for seeds, core-shell and modified $CoFe_2O_4$-ZnO core-shell nanoparticles were 60.9

$mM^{-1}s^{-1}$, 31.8 $mM^{-1}s^{-1}$ and 264.6 $mM^{-1}s^{-1}$ respectively. It can be observed that between the two different core-shell geometries, the value of the transverse relaxivity of the protons is significantly higher for the modified core-shell geometry in which agglomerates of $CoFe_2O_4$ nanoparticles are contained in hollow ZnO spherical capsules. This significant increase in the transverse relaxivity value can be attributed to the presence of $CoFe_2O_4$ nanoparticles as agglomerates. It has been shown by researchers that if magnetic nanoparticles are close together and make agglomerates, magnetic spin moments are coupled to generate stronger magnetic fields. This 'magnetic coupling effect' directly influences the r_2 relaxivity and is expressed as:[32]

$$R2 = \frac{1}{T2} = \left(\frac{64\pi}{135}\right)\left(\mu N_g \frac{L(x)}{4\pi}\right)^2 \frac{N_A C_a}{R_a D} \quad (1)$$

Where, μ is magnetic moment of the nanoparticle, N_g is the number of nanoparticles in an agglomerate, C_a is the concentration of agglomerates, R_a is the radius of an agglomerate, D is the water diffusion coefficient, N_A is the Avogadro's number, and $L(x)$ is the Langevin function.

Since the core-shell and modified core-shell nanoparticles have ZnO coating over them they can be used as contrast agents for fluorescence imaging as well. The images recorded under blue, green and red emission along with the control in the presence of core-shell and modified core-shell nanoparticles are shown respectively in Fig. 8(a) and (b). It can be observed in Fig. 8 that the control that does not contain any nanoparticles is not showing any cells in fluorescence images. Whereas, cells containing nanoparticles are visible in blue, green and red emission.

UV-Visible spectra obtained from core-shell and modified core-shell nanoparticles are shown in Fig. 9(a). A broad peak at ~360 nm corresponding to the absorption band of ZnO can be observed for both the core-shell geometries. The large peak broadness can be attributed to the strong surface coupling between the ZnO with $CoFe_2O_4$ phases. PL spectra obtained from core-

shell and modified core-shell nanoparticles are shown in Fig. 9(b). The emission spectrum for both samples was recorded by excitation at 240 nm. Both the samples exhibited a broad emission band and a small hump near 530 nm due to oxygen vacancy and surface defects.

To investigate the cytotoxicity of the core-shell and modified $CoFe_2O_4$-ZnO core-shell nanoparticles, MTT assay was performed using MCF-7 (human Brest cancer cells). Iron concentration of the chitosan coated nanoparticle dispersion was determined by AAS (Atomic Absorption Spectroscopy). For MTT analysis the chitosan coated core-shell nanoparticle water dispersions were used. Results from the cytotoxicity experiment shown in Fig. 10 clearly reveal that the core shell and modified $CoFe_2O_4$-ZnO core-shell nanoparticles with different concentrations (100, 50, 25, 12.5 and 6.25 μg/mL) are bio-compatible towards the MCF-7 cell line.

4. Conclusion

This work clearly demonstrates (a) the potential of $CoFe_2O_4$-ZnO core-shell nanoparticles as contrast agent for optical fluorescence imaging and MRI and (b) the effect of particle agglomeration induced coupling of magnetic spin moments on enhancing the proton relaxivity value during the NMR experiment. $CoFe_2O_4$-ZnO nanoparticles with two different core-shell geometries were synthesized and examined. In one case, individual core-shell nanoparticles contained $CeFe_2O_4$ as core and ZnO as shell. Whereas, in the other case, large agglomerates of $CoFe_2O_4$ nanoparticles were encapsulated within hollow ZnO capsules. This alteration in the core-shell configuration was made possible by changing the surfactant chemistry during the nanoparticle synthesis process. The core-shell geometry in which $CoFe_2O_4$ nanoparticle agglomerates were present within ZnO capsules yielded a very high value of transverse proton relaxivity when compared to the proton relaxivity value exhibited by the individual core-shell

nanoparticles. During the fluorescence imaging experiment, the cells containing the core-shell nanoparticles were visible in blue, green and red emission whereas the control sample (cells without nanoparticles) yielded a completely dark image. The Fluorescent $CoFe_2O_4$-ZnO core-shell nanoparticles exhibited biocompatibility towards the MCF-7 cell line.

5. Acknowledgement

Authors acknowledge the electron microscopy facilities available at the Advanced Centre for Microscopy and Microanalysis (AFMM) IISc Bangalore. The MCF-7 cell line were provided by Professor Paturu Kondaiah. Cell toxicity analysis was done using the facilities available in Professor Paturu Kondaiah's laboratory in IISc, Bangalore. C. Srivastava acknowledges the research grant received from Department of Science and Technology DST-Nano Mission and SERB, Govt. of India. The NMR facility at NMR Research Centre, supported by DST, is gratefully acknowledged.

References

1 A. R. Kherlopian, T. Song, Q. Duan, M. A. Neimark, M. J. Po, J. K. Gohagan and A. F. Laine, *BMC Syst. Biol.*, 2008, **2**, 1752-74.

2 L. Fass, *Mol. Oncol.*, 2008, **2**, 115–152.

3 K. Glunde, A. P. Pathak and Z. M. Bhujwalla, *Trends in Mol. Med.*, 2007, **13**, 287–297.

4 T.H. Shin, Y. Choi, S. Kim and J. Cheon, *Chem. Soc. Rev.*, 2015, **44**, 4501–4516.

5 J. Zheng, G. Perkins, A. Kirilova, C. Allen and D. A. Jaffray, *Invest. Radiol.*, 2006, **41**, 339–348.

6 P. Sharma, A. Singh, S. C. Brown, N. Bengtsson, G. A. Walter, S. R. Grobmyer, N. Iwakuma, S. Santra, E. W. Scott and B. M. Moudgil, *Methods Mol. Biol.*, 2010, **624**, 67–81.

7 Q. L. Trequesser, H. Seznec and M.H. Delville, *Nanotechnol. Rev.*, 2013, **2**, 125–169.

8 J. E. Lee, N. Lee, H. Kim, J. Kim, S. H. Choi, J. H. Kim, T. Kim, I. C. Song, S. P. Park, W. K. Moon and T. Hyeon, *J. Am. Chem. Soc.*, 2010, **132**, 552–557.

9 X.-P. Y. Peng Wu, *Chem. Soc. Rev.*, 2013, **42,** 4859-4866.

10 P. Tallury, S. Santra, P. Sharma, B. M. D. C. Matos, N. Bengtsson, S. Biswas, A. K. Saha, G. A. Walter, E. A. Scott and B. M. Moudgil, *J. Biomed. Nanotechnol.*, 2011, **7**, 724–729.

11 A. Maiseyeu, G. Mihai, T. Kampfrath, O. P. Simonetti, C. K. Sen, S. Roy, S. Rajagopalan and S. Parthasarathy, *J. Lipid Res.*, 2009, **50**, 2157–2163.

12 C. Fang and M. Zhang, *J. Control. Release*, 2010, **146**, 2–5.

13 B. P. Joshi and T. D. Wang, *Cancers*, 2010, **2**, 1251–1287.

14 L. Chen, Y. Shen, J. Bai, *Mat. Lett*., 2009, 63, 1099-1101.

15 Y. Yuan, L. Chen, R. Yang, X. Lu, H. Peng, Z. Luo, *Mat. Lett.*, 2012, 71, 123-126.

16 L. Chen, H. Dai, Y. Shen, J. Bai, *J. Alloys Compd.*, 2010, 491, L33-L38.

17 H. B. Na, I. C. Song and T. Hyeon, *Adv. Mater.*, 2009, **21**, 2133–2148.

18 S. Laurent, D. Forge, M. Port, A. Roch, C. Robic, L. V. Elst and R. N. Muller, *Chem. Rev.*, 2008, **108**, 2064–2110.

19 N. Venkatesha, C. Srivastava and V. Hegde, *IET Nanobiotechnol.*, 2013, **8**, 184–189.

20 Y. Zhang, T. R. Nayak, H. Hong and W. Cai, *Curr. Mol. Med.*, 2013, **13**, 1633–1645.

21 Y. Liu, K. Ai, Q. Yuan and L. Lu, *Biomaterials*, 2011, **32**, 1185–1192.

22 A. L. Cruz, C. Barrera, V. L. C. Ddelc and C. Rinaldi, *J. Mater. Chem.*, 2009, **19**, 6870-6876.

23 E. S. Costa, M. M. Pereira and H. S. Mansur, *J. Mater. Sci. Mater. Med.*, 2008, **20**, 553–561.

24 H. Gunther, *NMR Spectroscopy: Basic Principles, Concepts and Applications in Chemistry*, John Wiley & Sons, 2013.

25 L. Zhao, H. Zhang, Y. Xing, S. Song, S. Yu, W. Shi, X. Guo, J. Yang, Y. Lei and F. Cao, *J.*

Solid State Chem., 2008, **181**, 245–252.

26 Y. T. Prabhu, K. V. Rao, V. S. S. Kumar and B. S. Kumari, 2013, **2,** 45-50.

27 R. O. Moussodia, L. Balan, C. Merlin, C. Mustin and R. Schneider, *J. Mater. Chem.*, 2010, **20**, 1147–1155.

28 S. M. Hoque, C. Srivastava, N. Srivastava, N. Venkateshan and K. Chattopadhyay, *J. Mater. Sci.*, 2013, **48**, 812–818.

29 H. Wang, L. Xin, H. Wang, X. Yu, Y. Liu, X. Zhou and B. Li, *RSC Adv.*, 2013, **3**, 6538–6544.

30 F. Bensebaa, F. Zavaliche, P. L. Ecuyer, R. W. Cochrane and T. Veres, *J. Colloid Interface Sci.*, 2004, **277**, 104–110.

31 R. R. Prabhakar, N. Mathews, K. B Jinesh, K. R. G. Karthik, S. S. Pramana, B. Varghese, C. H. Sow and S. Mhaisalkar, *J. Mater. Chem.*, 2012, **22**, 9678–9683.

32 Q. L. Vuong, P. Gillis and Y. Gossuin, *J. Magn. Reson.*, 2011, **212**, 139–148.

Figure captions:

Fig. 1 SEM-EDS profile obtained from (a) $CoFe_2O_4$ seeds, (b) core-shell and (c) modified core-shell $CoFe_2O_4$-ZnO nanoparticles.

Fig. 2 XRD profiles obtained from $CoFe_2O_4$ seeds, core-shell and modified core-shell $CoFe_2O_4$-ZnO nanoparticles.

Fig. 3 (a) TEM bright field image and SAD pattern obtained from $CoFe_2O_4$ seeds, (b) size distribution histogram of $CoFe_2O_4$ seeds, (c) TEM bright field image (insert showing high resolution TEM image), (d) Size distribution histogram, (e) SAD pattern obtained from $CoFe_2O_4$-ZnO core-shell nanoparticles, (f) STEM-HAADF image of $CoFe_2O_4$-ZnO core shell nanoparticle; Compositional profile (obtained along AB marked in figure 3(f)) for (g) Co and (h) Fe.

Fig. 4 (a) low magnification and (b) high magnification TEM bright field image of modified core-shell $CoFe_2O_4$-ZnO nanoparticles, (c) SAD pattern from the capsules containing nanoparticles agglomerates, (d) SAD pattern obtained from a capsule containing very less number of nanoparticles, (e) STEM-HAADF image of capsules containing nanoparticle agglomerates and (f) EDS profile obtained from the red region marked in figure 4(e).

Fig. 5 XPS spectrum showing peaks corresponding to Co, Fe, Zn and O obtained from modified core-shell $CoFe_2O_4$-ZnO nanoparticles.

Fig. 6 Magnetic hysteresis curves for $CoFe_2O_4$ seeds, core-shell and modified core-shell $CoFe_2O_4$-ZnO nanoparticles.

Fig.7 $1/T_2$ vs. Fe concentration plot for (a) $CoFe_2O_4$ seeds, (b) core-shell and (c) modified core-shell $CoFe_2O_4$-ZnO nanoparticles.

Fig. 8 Fluorescence images of Hela cells incubated with (a) core-shell and (b) modified core-shell $CoFe_2O_4$-ZnO nanoparticles.

Fig. 9 (a) UV-visible absorption and (b) PL spectra obtained from the core-shell and modified core-shell nanoparticles.

Fig. 10 MTT assays of (a) $CoFe_2O_4$-ZnO core-shell nanoparticles and (b) modified $CoFe_2O_4$-ZnO core-shell nanoparticles.

Figure 1.

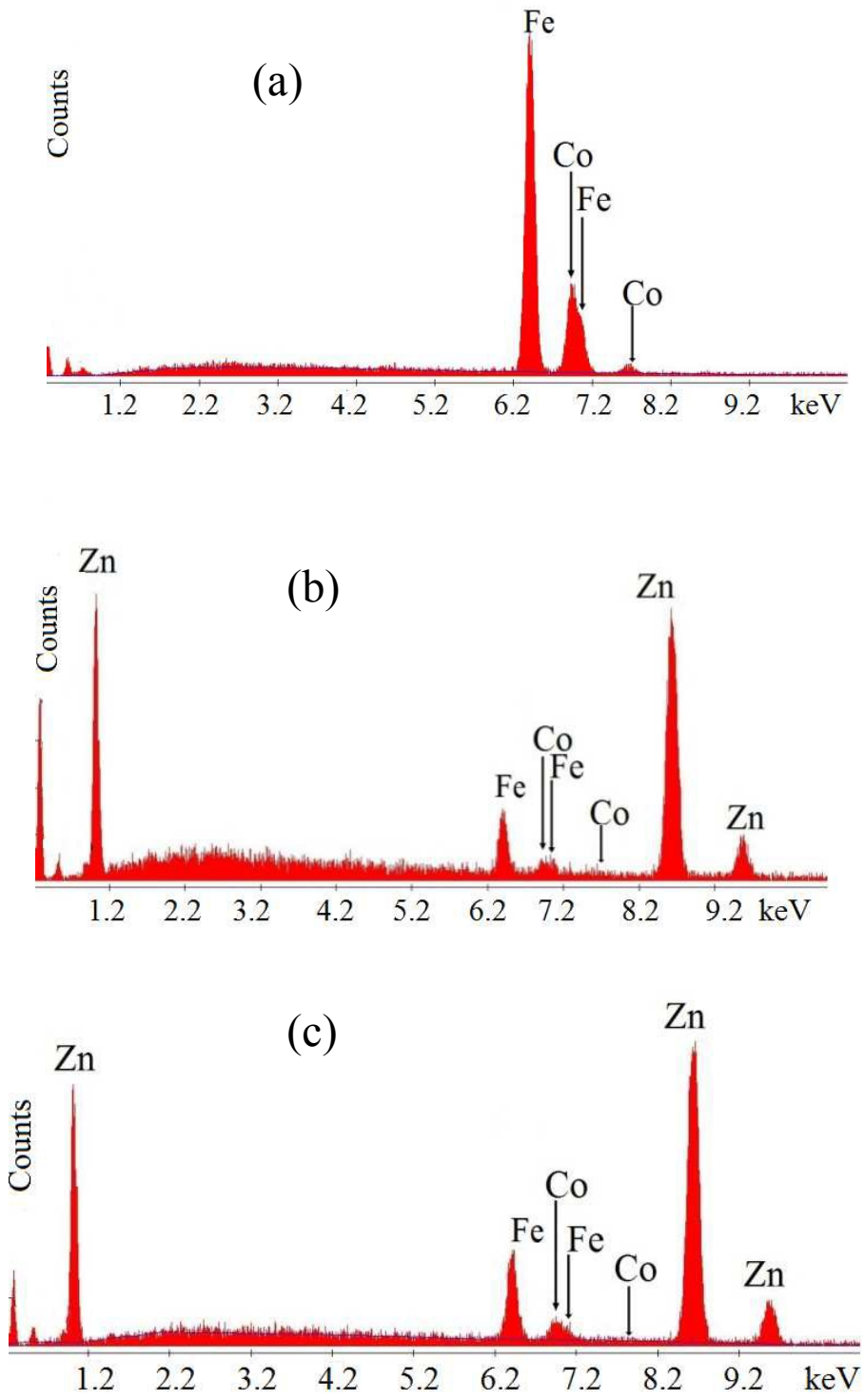

Figure 2.

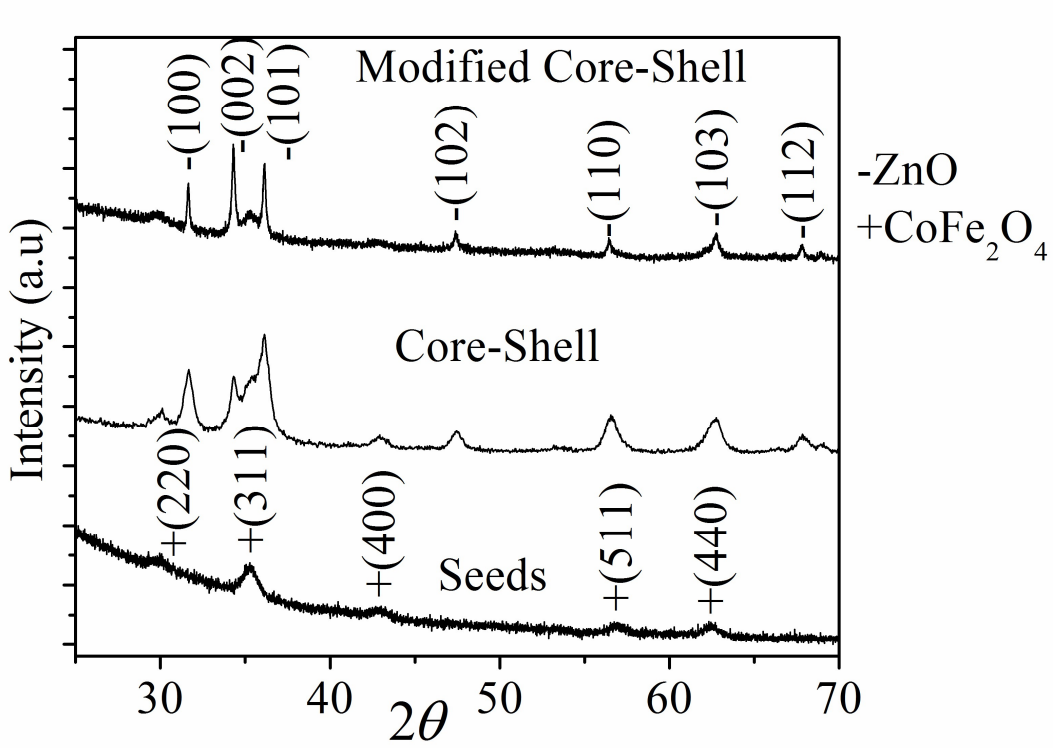

Figure 3

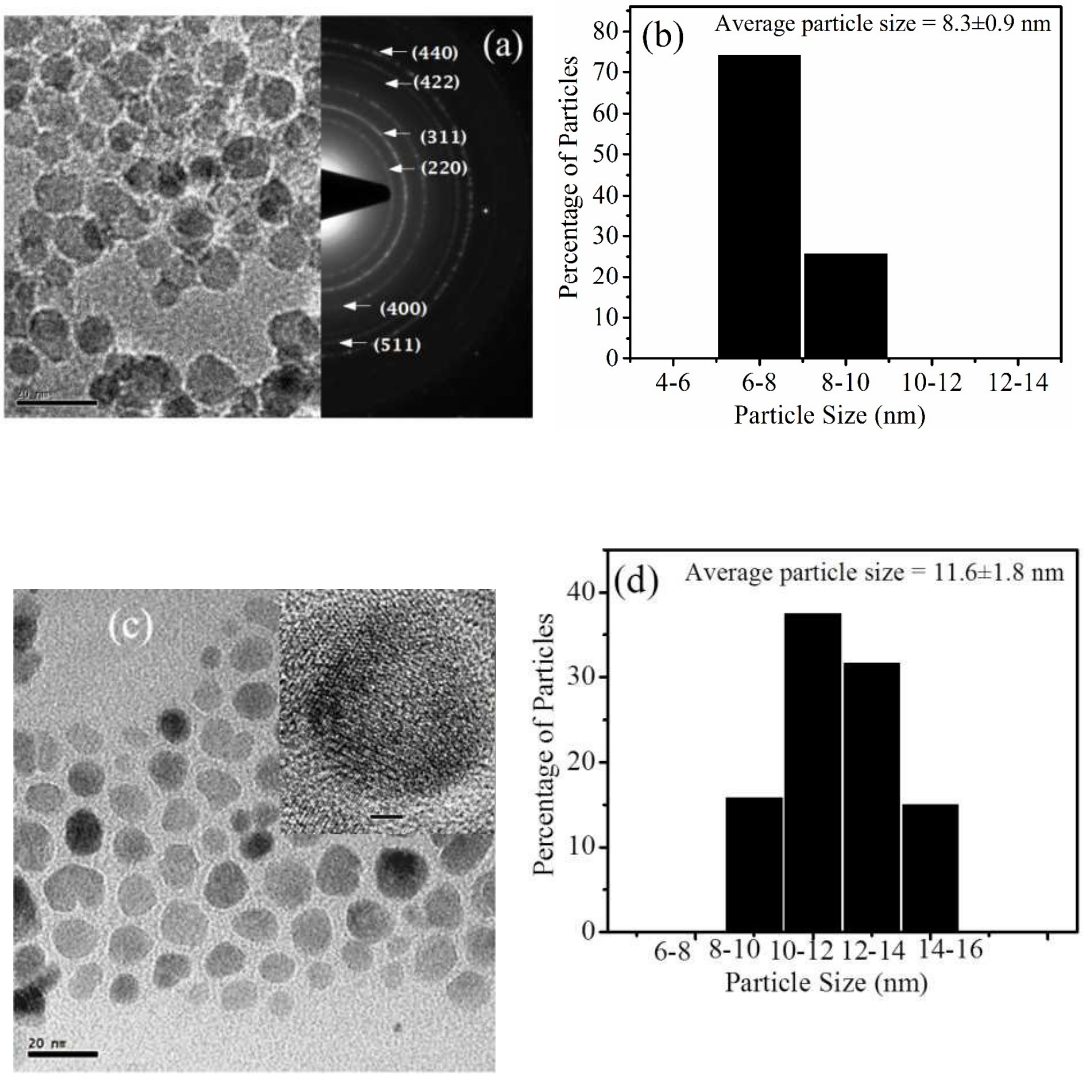

Figure 3

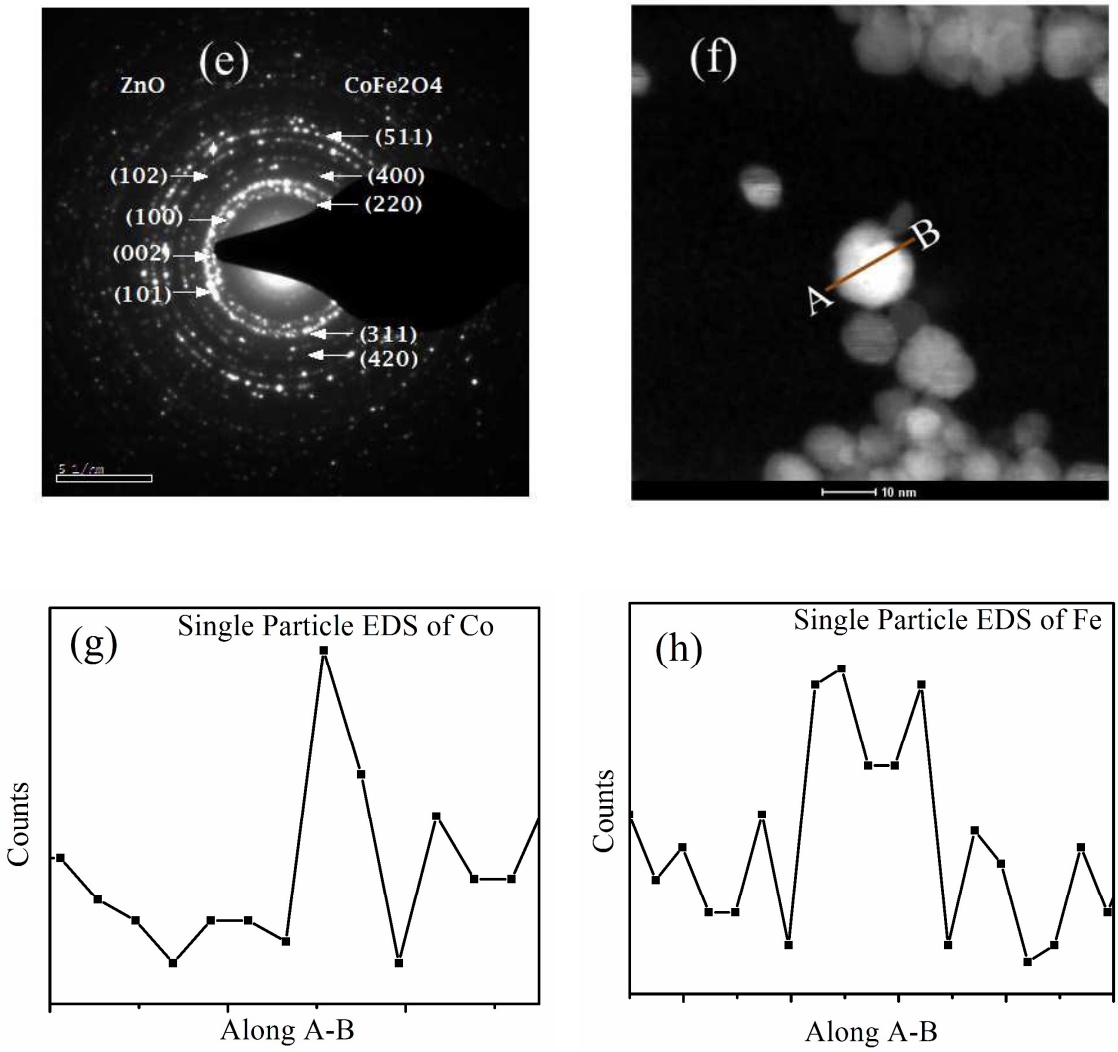

Figure 4.

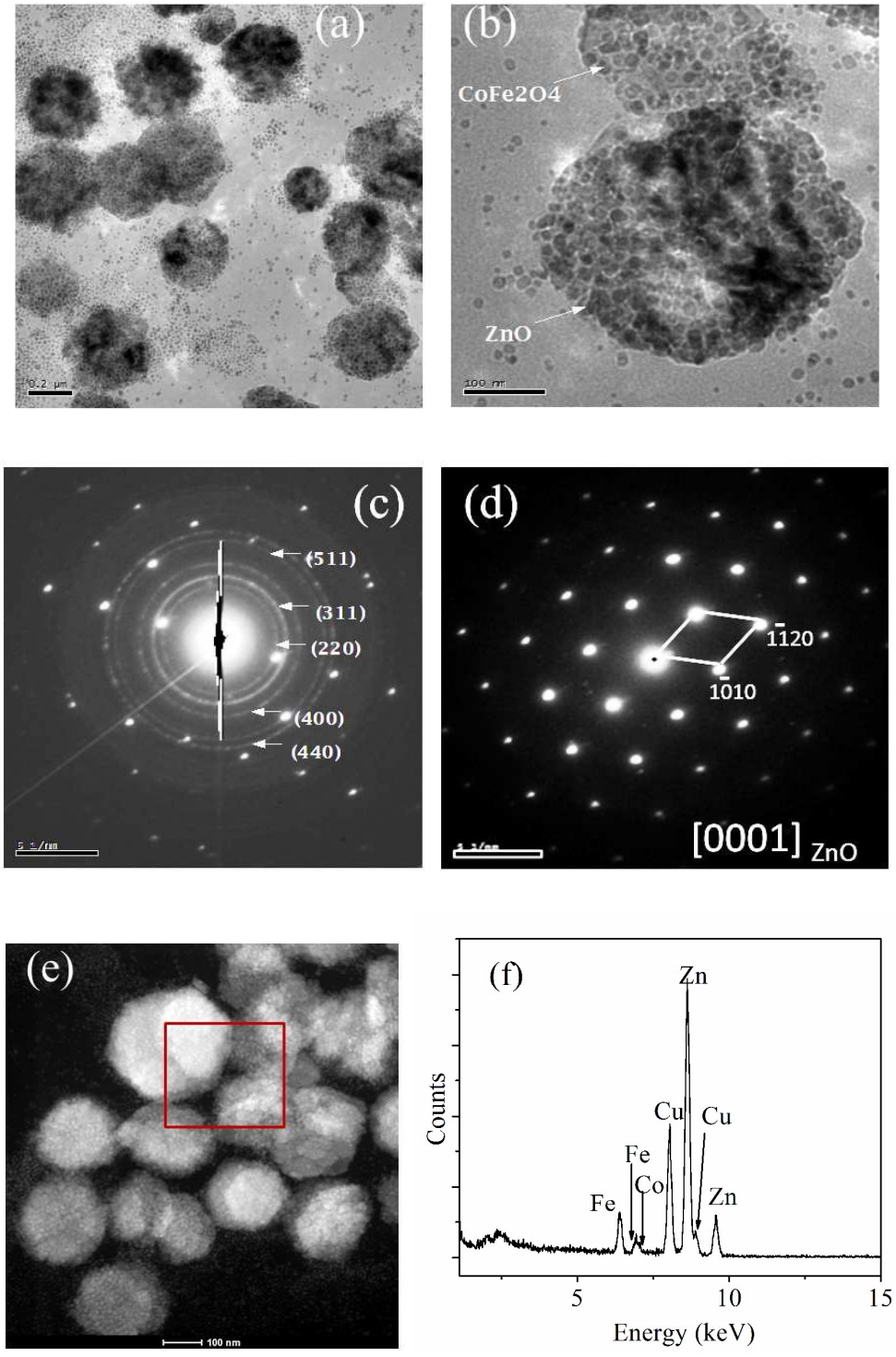

Figure 5.

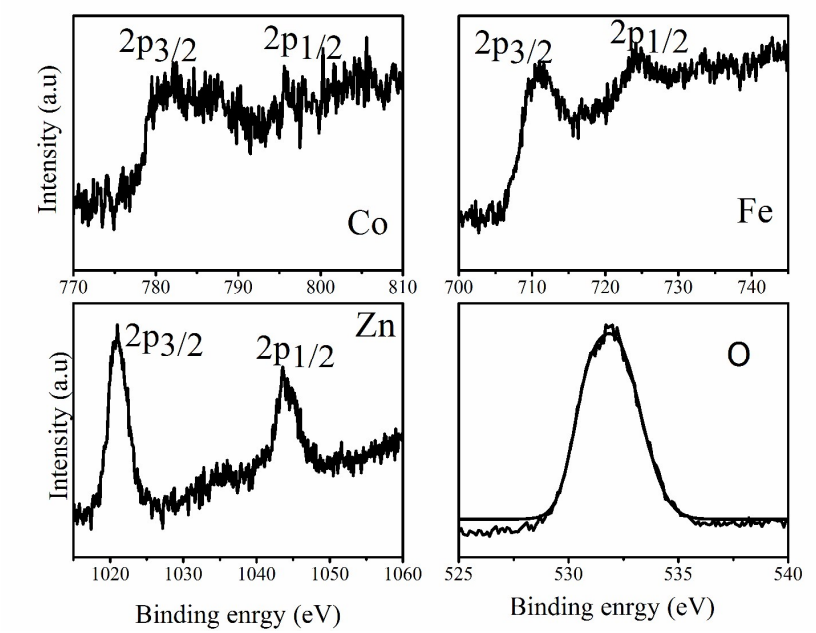

Figure 6.

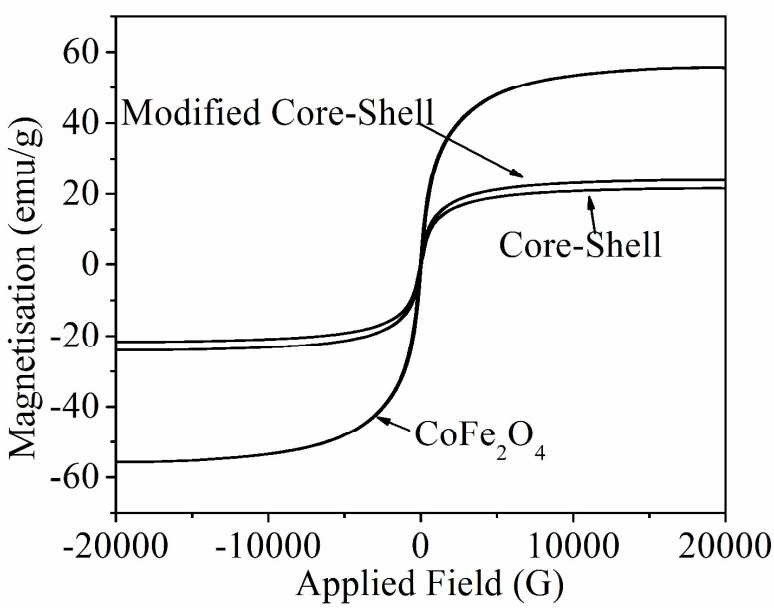

Figure 7.

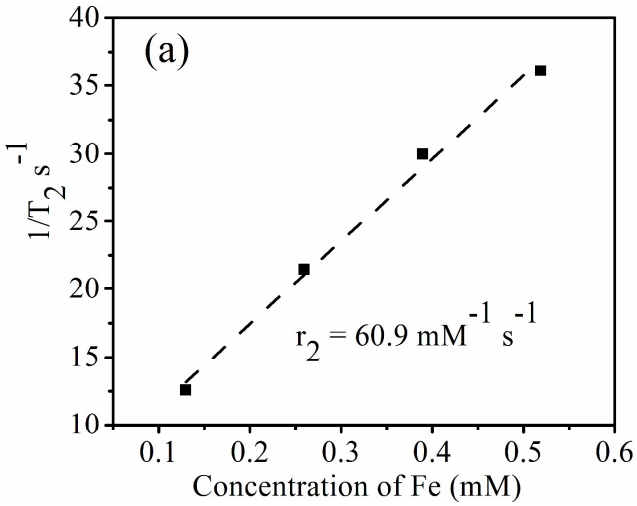

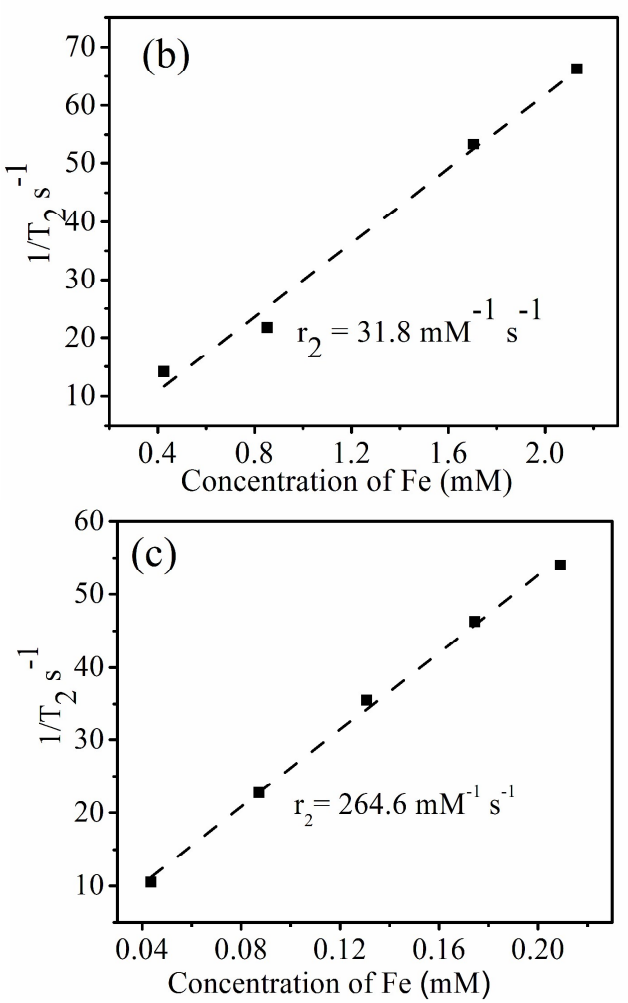

Figure 8.

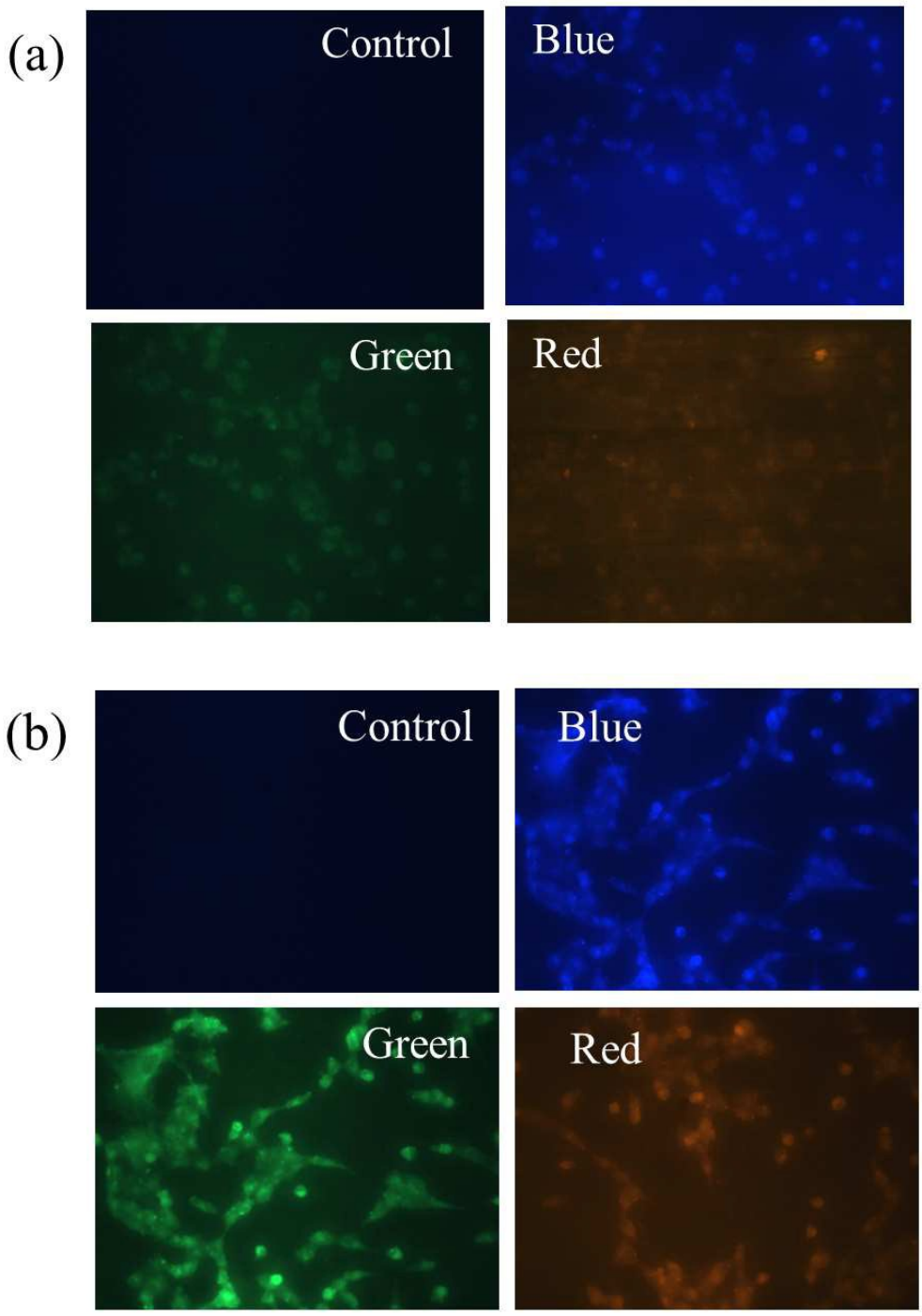

Figure 9

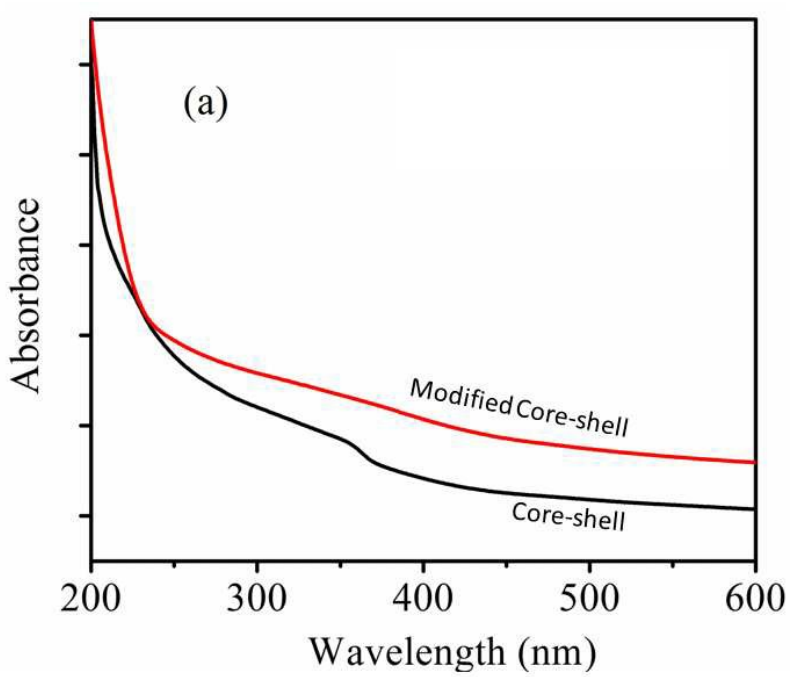

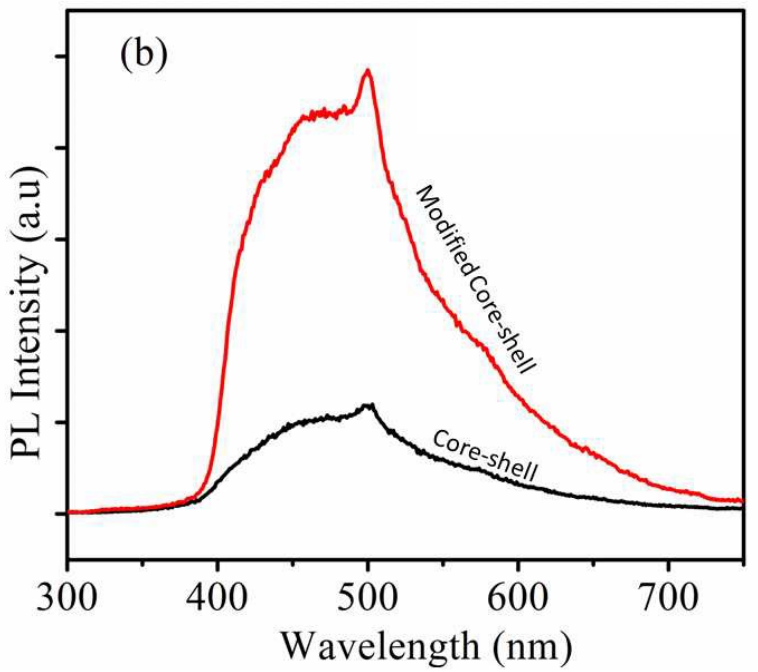

Figure 10.